Li^+ Transport in Lithium Sulfonylimide−Oligo(ethylene oxide) Ionic Liquids and Oligo(ethylene oxide) Doped with LiTFSI

Oleg Borodin,*,† G. D. Smith,† Olt Geiculescu,‡ Stephen E. Creager,‡ Boutros Hallac,‡ and Darryl DesMarteau‡

Department of Materials Science & Engineering, 122 South Central Campus Drive, Room 304, University of Utah, Salt Lake City, Utah 84112-0560, and Department of Chemistry, Clemson University, Clemson, South Carolina 29634

Received: August 16, 2006

The Li^+ environment and transport in an ionic liquid (IL) comprised of Li^+ and an anion of bis-(trifluoromethanesulfonyl)imide anion ($TFSI^-$) tethered to oligoethylene oxide (EO) ($EO_{12}TFSI^-/Li^+$) were determined and compared to those in a binary solution of the oligoethylene oxide with LiTFSI salt (EO_{12}/LiTFSI) by using molecular dynamics (MD) simulations and AC conductivity measurements. The latter revealed that the AC conductivity is 1 to 2 orders of magnitude less in the IL compared to the oligoether/salt binary electrolyte with greater differences being observed at lower temperatures. The conductivity of these electrolytes was accurately predicted by MD simulations, which were used in conjunction with a microscopic model to determine mechanisms of Li^+ transport. It was discerned that structure-diffusion of the Li^+ cation in the binary electrolyte (EO_{12}/$LiTFSI^-$) was similar to that in $EO_{12}TFSI^-/Li^+$ IL at high temperature (>363 K), thus, one can estimate conductivity of IL at this temperature range if one knows the structure-diffusion of Li^+ in the binary electrolyte. However, the rate of structure-diffusion of Li^+ in IL was found to slow more dramatically with decreasing temperature than in the binary electrolyte. Lithium motion together with EO_{12} solvent accounted for 90% of Li^+ transport in EO_{12}/$LiTFSI^-$, while the Li^+ motion together with the $EO_{12}TFSI^-$ anion contributed approximately half to the total Li^+ transport but did not contribute to the charge transport in IL.

I. Introduction

For lithium batteries to meet requirements for use in hybrid and electric vehicles electrolytes with improved safety and ion transport must be developed. Solid polymer electrolytes (SPEs), gel electrolytes, and ionic liquids (ILs) are being widely investigated for use in various types of lithium batteries as alternatives to traditional liquid electrolytes based on mixtures of carbonates.[1] SPEs combine ease of fabrication, good electrochemical stability, low flammability, and toxicity with the ability to form good interfacial contact with electrodes during charge−discharge cycles, and eliminate a need for a separator. Despite these advantages over liquid electrolytes, current SPEs exhibit low ambient temperature conductivity and low lithium transference numbers preventing them from being used in batteries for consumer electronics and automotive applications.[1] Plasticizing SPEs with traditional carbonate solvents, forming gel electrolytes, has resulted in improved ion transport but poor mechanical properties and high solvent volatility. The most widely investigated ILs are organic salts with low melting points (typically at or below room temperature) based on pyrrolidinium and imidazolium cations (with an associated anion) doped with Li salts.[2] These electrolytes are potential replacements for volatile carbonate electrolytes due to the expected improvements in battery safety and electrochemical stability while providing sufficient Li^+ cation transport. Plasticizing SPEs with nonvolatile ILs creates gels with no volatile components but low lithium transport.[3]

All the electrolytes discussed above have a (nonionic) mobile solvent component and/or mobile anions, and hence a transference number $t^0_+ < 1$, leading to development of concentration polarization during battery operation that significantly limits battery performance.[4] Modeling has shown that electrolyte systems with a unity transference number have improved performance over systems with transference numbers of 0.2−0.3 even when the conductivity is decreased by an order of magnitude.[4] Elimination of the mobile anion by covalent attachment to a polymer chain (single ion conductor) or use of ILs (molten salts) that contain only lithium and anion and no solvent eliminates performance problems associated with salt concentration polarization. Unfortunately, single ion conductors typically exhibit much lower conductivity than binary electrolytes.[5−9]

The details of the synthesis and characterization of a series of ionic liquids consisting of lithium fluorosulfonimide salts in which the fluorosulfonimide anion is covalently attached to a lithium-solvating polyether chain via a fluorinated ether linkage are reported elsewhere.[10] The detailed structure of one member of this family of ionic liquids having an average of 11.8 ethylene oxide units in the polyether chain bound to the fluorosulfonimide anion is given in Table 1. In the following discussion we designate this ionic liquid as EO_nTFSI^-/Li^+ to indicate that it consists of an oligomeric ethylene oxide (EO) chain bonded to a fluorosulfonimide anion similar in structure to the bis-(trifluoromethanesulfonyl)imide ($TFSI^-$) anion. The EO_nTFSI^-/Li^+ IL has potential to offer higher conductivity compared to

* Address correspondence to this author. E-mail: oleg.borodin@utah.edu.
† University of Utah.
‡ Clemson University.

10.1021/jp0653104 CCC: $33.50
Published on Web 11/09/2006

TABLE 1: Structure of Electrolytes Used in Experimental Measurements and MD Simulations

abbreviated notation	chemical formula	used in
EO_n/LiTFSI	$CH_3O(CH_2CH_2O)_{n-1}CH_3$ doped $Li^+(CF_3SO_2NSO_2CF_3)^-$	MD and expt
EO_nTFSI^-/Li^+	$(CH_3O\text{-}(EO)_{n-1}\text{-}CF_2CFHOCF_2\text{-}CF_2SO_2NSO_2CF_3)^-/Li^+$	expt
EO_nTFSI^-/Li^+	$(CH_3O(CH_2CH_2O)_{n-1}CH_2CF_2\text{-}SO_2NSO_2CF_3)^-/Li^+$	MD

polymeric single ion conductors[6−8,11,12] that have anion tethered to a polymer chain.

The $TFSI^-$ anion is one of the most popular large anions in lithium battery technology with of one of the lowest binding energies to Li^+. Ionic liquids based on lithium fluorosulfonimide salts are therefore expected to provide a high degree of ion Li^+/anion dissociation and, therefore, improved conductivity compared to the previously used ionic liquids with sulfonate anion[13] or sulfate ester[14] attached to oligoethers. The oligo(ethylene oxide) solvating host is also expected to provide better salt dissociation and lithium transport compared to oligo(propylene oxide) (PO) used in previous PO_nAnion^-/Li^+ ionic liquids.[13,15] Finally, the structure of the fluorosulfonimide anion used in our studies is different from that of fluorosulfonamides (fluorosulfonamide = alkyl-N-SO_2CF_3, with only one fluorosulfonyl group bound to nitrogen) that have been used in previous studies.[16−19] Specifically, in the materials considered here there are two fluoroalkylated sulfonyl groups attached to the imide nitrogen, which is essential to providing the charge delocalization that gives rise to the low lattice energy and high dissociation of the lithium fluorosulfonimide salts. Other workers have focused on fluorosulfonamides which have only a singly fluoroalkylated sulfonyl group attached to nitrogen.[16] Fluorosulfonamide anions have less extensive negative charge delocalization relative to fluorosulfonimide anions, and so fluorosulfonamide salts are less likely to exhibit the high salt dissociation that is needed to achieve high conductivity

In this work we present the results of molecular dynamics (MD) simulations on lithium-conducting ionic liquid electrolytes that are similar to (albeit slightly different from) the materials that were the subject of our recent report.[10] We focus on obtaining fundamental understanding of the mechanism of Li^+ transport in $EO_{12}TFSI^-/Li^+$ IL in comparison with a liquid electrolyte comprised of the oligoether doped with LiTFSI salt (EO_{12}/LiTFSI). In this binary electrolyte the anion is not attached to the oligoether and hence is highly mobile. We are particularly interested in how Li^+ transport changes upon attachment of $TFSI^-$ anion to oligoether and the possibility of estimating conductivity of IL from detailed knowledge of the Li^+ transport mechanism in its binary electrolyte counterpart. The paper is organized as follows: in Section II we present experimental conductivity measurements obtained on the $EO_{13}TFSI^-/Li^+$ ionic liquid (which were first presented in our recent report describing synthesis and characterization of these electrolytes) and also on a EO_{12}/LiTFSI binary salt electrolyte prepared by dissolving LiTFSI and the liquid polyether solvent. Molecular dynamics simulation methodology is presented in Section III. Analysis of the Li^+ environment and transport properties is presented in Sections IV and V. In Section VI we parametrize a microscopic model for Li^+ transport and utilize this model in conjunction with analysis of MD simulations to discern mechanisms of Li^+ transport and bottlenecks limiting conductivity of $EO_{12}TFSI^-/Li^+$ ILs.

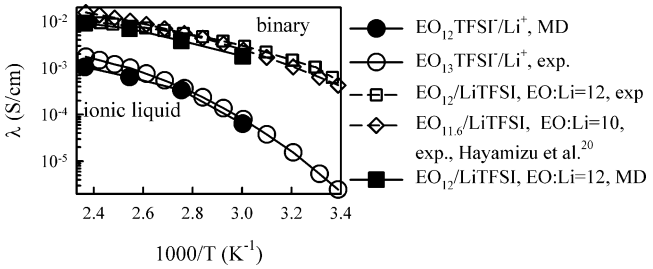

Figure 1. Conductivity of EO_{12}/LiTFSI binary electrolyte and EO_n-$TFSI^-/Li^+$ IL from MD simulations ($n = 12$) and experiments ($n = 13$). Hayamizy data are from ref 20.

II. Conductivity Measurements

The ionic liquid with the structure $CH_3O\text{-}(CH_2CH_2O)_{n-1}\text{-}CF_2\text{-}CFHOCF_2CF_2SO_2NSO_2CF_3/Li^+$, $n = 12.8$, denoted as EO_{13}-$TFSI^-/Li^+$ was synthesized and characterized as discussed in detail elsewhere. Number-average molecular weight for the IL was determined by NMR end-group analysis to be consistent with an average of 11.8 ether oxygen repeat units per salt equivalent. The polydispersity index was low (less than 1.2) as determined by electrospray ionization mass spectrometry measurements. Details are provided in our separate report.[10] Binary salt electrolytes were prepared by dissolving lithium bis-(trifluoromethylsulfonyl)imide salt (LiTFSI obtained from 3M) in liquid poly(ethylene oxide) dimethoxy ether (PEGDME, obtained from Aldrich) having a number-average molecular weight of 486 Da (corresponding to an average of 10 EO units per chain) and a weight-average molecular weight of 500 Da (corresponding to a polydispersity index of 1.03). Conductivity measurements on both electrolytes were performed by electrochemical impedance spectroscopy, using a cell in which an electrolyte layer is interposed between two stainless steel blocking electrodes. Details are given in our prior report.[10]

Temperature dependence of conductivity of $EO_{13}TFSI^-/Li^+$ ionic liquid is compared in Figure 1 with temperature dependence of a binary EO_{12}/LiTFSI electrolyte at EO:Li = 12 that was prepared and studied in this work, and also with previously reported measurements by Hayamizu[20] for $CH_3\text{-}EO_{10.6}\text{-}OCH_3$/LiTFSI also denoted as EO_{12}/LiTFSI at salt concentrations of EO:Li = 10. The two data sets for binary EO_{12}/LiTFSI electrolytes from different sources and for slightly different EO:Li ratios are in good agreement with each other. Figure 1 shows that attaching $TSFI^-$ anion to oligoether reduces electrolyte conductivity by an order of magnitude at high temperatures and up to 2 orders of magnitude at room temperature. This finding highlights a key fundamental difference between binary salt-in-solvent electrolytes and ionic liquid electrolytes.

III. Molecular Dynamics Simulation Methodology

MD simulations were performed on $CH_3O(CH_2CH_2O)_{n-1}$-CH_3/LiTFSI, $n = 12$, binary electrolyte denoted as EO_{12}/LiTFSI at EO:Li = 12 salt concentration and $EO_{12}TFSI^-/Li^+$ IL with the chemical structure shown in Table 1. Simulations were performed at temperatures from 333 to 423 K as shown in Table 2. Note that the simulated EO_nTFSI^-/Li^+ IL has a slightly lower degree of polymerization ($n = 12$) compared to that for the experimentally synthesized samples ($n = 13$) because at the time when MD simulations were initiated the precise molecular weight of experimental samples was not known.

A version of the MD simulation package Lucretius[21] that includes many-body polarization was used for all MD simula-

TABLE 2: Length of MD Simulations, Fractions of Free Ions α_s ($r_{Li-N} > 5$ Å), and Degree of Ion Uncorrelated Motion (α_d)

temp (K)	run length (ns) equilibration	run length (ns) production	density (kg m^{-3})	α_s	α_d	r_{jump} (ns^{-1})
			EO_{12}/LiTFSI			
423	3	30	1169	0.79	$0.7_5 \pm 0.15$	24
393	2	15.5	1190	0.80	$0.8_3 \pm 0.15$	13
363	2	35	1225	0.84	$0.8_9 \pm 0.15$	
333	1.5	13.4	1258	0.9	0.9 ± 0.15	
			$EO_{12}TFSI^-/Li^+$			
423	3	25	1209	0.78	$0.4_5 \pm 0.15$	16
393	2	8	1231	0.82	$0.4_5 \pm 0.15$	5.3
363	2	15	1257	0.84	$0.4_7 \pm 0.15$	
333	2	27	1285	0.85	$0.5_5 \pm 0.15$	

tions. The many-body force field previously developed[22,23] was used. The three-dimensional, periodic cubic simulation cell consisted of 24 LiTFSI + 24 EO_{12} chains for binary electrolyte and 32 $EO_{12}TFSI^-$ + 32 Li^+ cations for the IL. All electrolytes were created in the gas phase corresponding to a cell (linear) dimension of approximately 100 Å. The cell was shrunk to the size corresponding to a density that yielded an average pressure of 1 atm over 0.5 ns at 423 K simulations, using Brownian dynamics. Simulations were first performed at 423 K. After approximately 40−60% of the trajectory at 423 K was generated the temperature was decreased to 393 K. The same procedure was repeated at 363 and 333 K. Table 2 summarizes the length of production and equilibration runs performed with NVT and NPT ensembles, respectively.

A Nośe-Hoover thermostat and a barostat were used to control the temperature and pressure with the associated frequencies 10^{-2} and 10^{-3} fs^{-1}. Bond lengths were constrained by using the Shake algorithm.[24] The Ewald summation method[24] was used for treatment of long-range electrostatic forces between permanent charges and between permanent charges and induced dipoles for the many-body polarizable potential. The Ewald convergence parameter α was set to 8 Å. The number of reciprocal space vectors was set to 6^3. A tapering function was used for scaling the induced dipole−induced dipole interactions to zero at the cutoff of 10 Å, with scaling starting at 9 Å. A multiple time step reversible reference system propagator algorithm[25] was employed, with a time step of 0.5 fs for bonding, bending, and torsional motions, a 1.5 fs time step for nonbonded interactions within a 6.5 Å sphere, and a 3.0 fs time step for nonbonded interactions between 6.5 and 10.0 Å and the reciprocal space part of the Ewald summation. Coordinates were stored every 1 ps, and stress tensor was stored every 12 fs.

IV. Electrolyte Density and Li^+ Environment

The densities for EO_{12}/LiTFSI and $EO_{12}TFSI^-/Li^+$ electrolytes are shown in Table 2. The density of the $EO_{12}TFSI^-/Li^+$ IL is about 3% greater than that of the EO_{12}/LiTFSI binary electrolyte, which can be attributed to elimination of free volume associated with the EO_{12} and $TFSI^-$ anion chain ends upon attaching a $TFSI^-$ anion to an oligoether.

We find that the Li^+ local environment in EO_{12}/LiTFSI and $EO_{12}TFSI^-/Li^+$ electrolytes is almost identical with that observed in previous simulations[26] of EO_{54}/LiTFSI SPE. Specifically, in EO_{12}/LiTFSI and $EO_{12}TFSI^-/Li^+$ IL each Li^+ cation has on average about 4.3 ether oxygens (EO) and 0.2 O^{TFSI-} within 2.8 Å, yielding a total of 4.5 oxygen atoms in the first close coordination shell of a Li^+ cation. This coordination is in good agreement with 4.9 oxygen atoms found coordinating each Li^+ cation in NDIS experiments of binary PEO/LiTFSI electrolyte EO:Li = 7.5.[27] When the radius of the Li^+ coordination shell is extended to 4 Å to include loosely coordinated ether oxygen atoms, each Li^+ is coordinated by about six ether oxygen atoms similarly to coordinations found in glyme$_2$/LiTFSI crystal structures.[28] We base all structural analyses reported in this paper on the close coordination shell of Li^+ using $r_{Li^+-O} < 2.8$ Å.

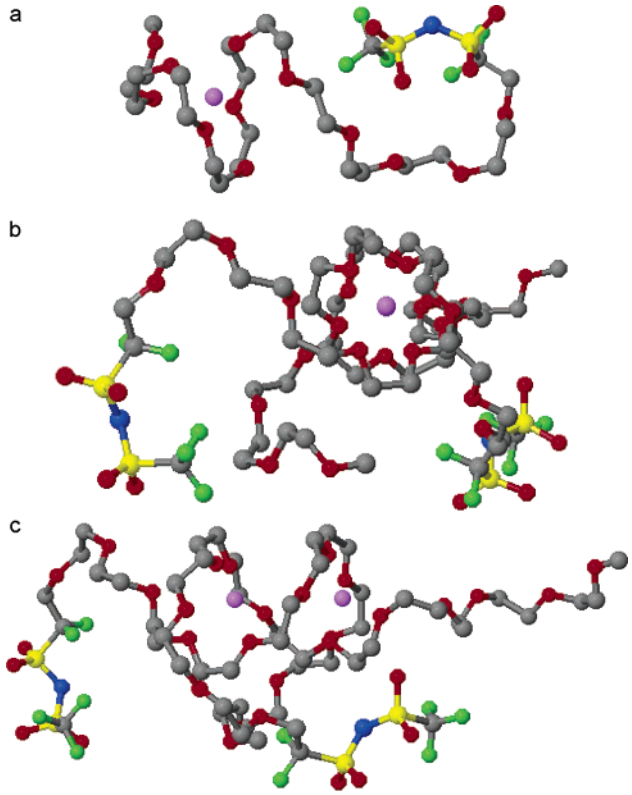

Figure 2. A Li^+ representative coordination by one (a) $EO_{12}TFSI^-$ and (b, c) two $EO_{12}TFSI^-$. Hydrogen atoms are not shown for clarity.

We find that approximately (50 ± 10)% of Li^+ cations are coordinated by one EO_{12} molecule or $EO_{12}TFSI^-$ anion as shown in Figure 2a, while the remaining Li^+ cations were coordinated by two EO_{12} molecules or two $EO_{12}TFSI^-$ anions. Approximately 15% of the Li^+ cations have another Li^+ cation, within 5.5 Å, a separation corresponding to the minima after the first peak of the Li^+-Li^+ radial distribution function. Such Li^+ cations are coordinated by two helical chains wrapping around Li^+ cations as shown in Figure 2b,c. Such structures could be stable for tens of nanoseconds at 393 and 423 K and do not allow lithium to efficiently move along a polymer chain resulting in a slower Li^+ transport by at least a factor of 2.5 compared to the Li^+ transport for structures coordinated by only 1 oligoether (Figure 2a).

The fraction of Li^+ cations separated from $TFSI^-$ anions by oligoether chains, denoted as α_s, is summarized in Table 2. In

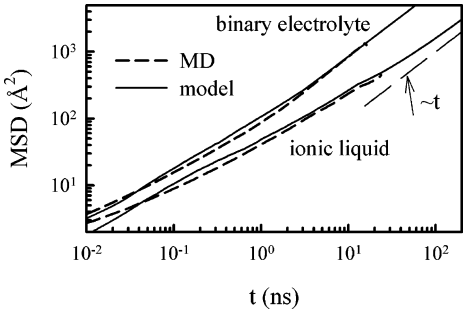

Figure 3. The Li^+ mean-square displacement (MSD) calculated directly from MD simulations and from microscopic model for EO_{12}/LiTFSI binary electrolyte and $EO_{12}TFSI^-/Li^+$ IL.

agreement with a spectroscopic study[29] of PEO/LiTFSI, we observe a high degree of cation−anion separation (dissociation), 75−90%, and essentially no difference between EO_{12}/LiTFSI binary electrolyte and $EO_{12}TFSI^-/Li^+$ IL. The degree of dissociation increases with decreasing temperature and is higher than the values observed at a similar salt concentration for other anions in previous simulations of Li-salt doped oligoether electrolytes.[26,30−34] We also find that when $Li^+/TFSI^-$ ion contact pairs are formed, a $TFSI^-$ anion donates only one oxygen atom to coordinate a Li.$^+$ Only one oxygen from each $TFSI^-$ anion coordinating a Li^+ cation was also found in X-ray studies[28,35] of glyme/$(LiTFSI)_2$ and LiTFSI crystals. Our previous simulations[36,37] of pyrrolidinium$^+TFSI^-$ doped with LiTFSI and EC/LiTFSI also found that essentially all of $TFSI^-$ anions donated only one oxygen atom to Li^+ coordination. This is in contrast to the results of gas-phase $Li^+/TFSI^-$ geometry optimization predicting Li^+ coordinated by two oxygen atoms from a $TFSI^-$ anion[23,38] highlighting the difference between gas-phase and condensed-phase results.

V. Transport Properties

A. Ion and Solvent Self-Diffusion Coefficients. The self-diffusion coefficient D_i for species i was calculated by using the Einstein relation[24]

$$D_i = \lim_{t\to\infty} D_i^{\mathrm{app}}(t) = \lim_{t\to\infty} \frac{\langle \mathrm{MSD}_i(t)\rangle}{6t} \qquad (1)$$

where $\mathrm{MSD}_i(t)$ is mean-square displacement of a molecule center-of-mass during time t, $\langle\ \rangle$ denotes an ensemble average, and $D_i^{\mathrm{app}}(t)$ is the time-dependent apparent diffusion coefficient. The Li^+ cation MSD(t) for EO_{12}/LiTFSI and $EO_{12}TFSI^-/Li^+$ IL at 423 K are shown in Figure 3. The Li^+ motion is subdiffusive, i.e., $\mathrm{MSD}(t) \approx t^{\gamma}$ with $\gamma < 1$, on a nanosecond time scale for IL. At times ~10 ns Li^+ motion becomes diffusive ($\gamma = 1$) for EO_{12}/LiTFSI and appears to be slightly subdiffusive on this time scale for the IL. The MSD(t) for EO_{12} and $EO_{12}TFSI^-$ are similar to those of Li^+ in the corresponding electrolyte. In contrast, the $TFSI^-$ anion in the binary electrolyte diffuses relatively rapidly and becomes diffusive on the time scale of a few nanoseconds or less.

As temperature decreases, longer simulations are required to reach the diffusive regime, especially for the oligoethers and Li^+ cations. Such simulations are very expensive using the many-body polarizable potentials we employed, thus posing significant difficulties for obtaining the ion self-diffusion coefficient at low temperatures. To estimate the ion self-diffusion coefficient as accurately as possible at low temperatures we followed our previous work[26,36] and assumed that $\mathrm{MSD}_i(t)$ at different temperatures can be superimposed by

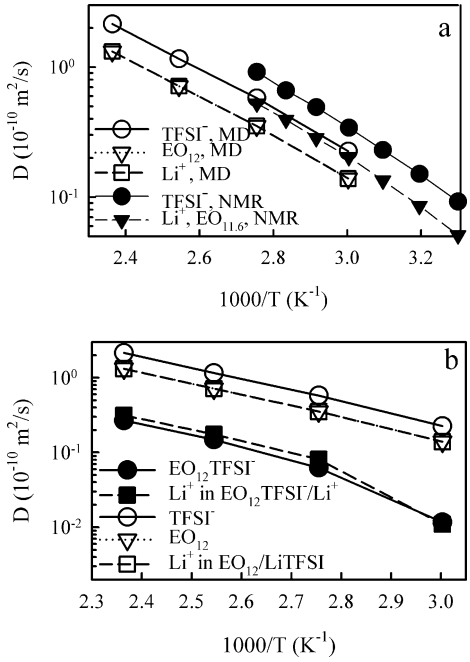

Figure 4. Solvent and ion self-diffusion coefficients for (a) EO_{12}/LiTFSI binary electrolyte from MD simulations and pgf-NMR experiments[20] and (b) comparison of self-diffusion coefficients for the binary electrolyte and IL from MD simulations.

scaling the time axis. The self-diffusion coefficients of all ions are determined as

$$D_i(T) = D_i(423\mathrm{K})/a_i(T) \qquad (2)$$

where D_i(423K) was obtained utilizing eq 1 at 423 K and $a_i(T)$ is the temperature-dependent time-shift factor obtained by superimposing $\mathrm{MSD}_i(t)$. Figure 4a shows a comparison of diffusion coefficients of Li^+, $TFSI^-$, and oligoether self-diffusion coefficients for EO_{12}/LiTFSI extracted from MD simulations with those from pgf-NMR measurements for a slightly lower molecular weight $EO_{11.6}$/LiTFSI at EO:Li = 10:1 salt concentration.[20] In both MD simulation and experiments the self-diffusion coefficients of $TFSI^-$ anion are 50−60% higher than those for the Li^+ cation and EO_{12} solvent. The absolute values of the ion and solvent self-diffusion coefficients from MD simulations are 35−40% lower than the corresponding values from pgf-NMR experiments.[20] We consider this agreement as good taking into account slightly lower molecular weight and some polydispersity of experimental samples, and the fact that the long range of hydrodynamic interactions compared to the simulation cell size restricts diffusion of liquids resulting in a smaller self-diffusion coefficient.[39] The later one can be estimated. The leading term of the finite size correction to the self-diffusion coefficient (ΔD^{FSC}) was found to be linearly proportional to the linear dimension of the simulation cell and is given by[39]

$$\Delta D^{\mathrm{FSC}} = \frac{2.837 k_{\mathrm{B}} T}{6\pi\eta L} \qquad (3)$$

where k_{B} is the Boltzmann constant, T is temperature, L is a linear dimension of the simulation periodic cell, and η is viscosity. We estimated viscosity of EO_{12}/LiTFSI at 423 and 393 K from simulations using the Einstein relation[22,40] to be 20 and 36 mPa s. Substituting these values into eq 3, we obtain ΔD^{FSC} values equal to 12% of the values for the EO_{12} self-diffusion coefficient, indicating that the finite size of the simulation cell results in approximately 12% reduction of the

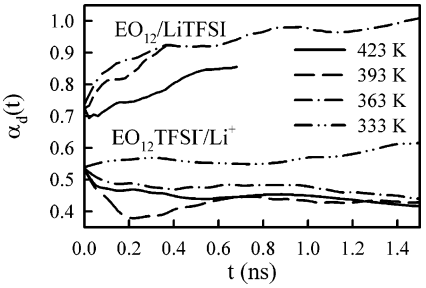

Figure 5. Degree of uncorrelated ion motion (α_d) for $EO_{12}TFSI^-/Li^+$ IL and EO/LiTFSI binary electrolyte from MD simulations.

solvent self-diffusion coefficient. We expect a similar effect for $EO_{12}TFSI^-/Li^+$ ionic liquid. Thus, the difference between pgf-NMR results[20] and MD simulation data corrected for the finite size effect of the simulation cell is only 22−27%. Figure 4b shows that the Li^+ self-diffusion coefficient in $EO_{12}TFSI^-/Li^+$ IL is approximately a factor of 5 smaller than that in EO_{12}/LiTFSI while diffusion of the $EO_{12}TFSI^-$ anion in the IL is a factor of 8−9 slower than diffusion of free $TFSI^-$ anion in the binary electrolyte.

B. Conductivity. Ionic conductivity can be calculated by MD simulations, using the Einstein relation[24]

$$\lambda = \lim_{t\to\infty} \lambda^{app}(t) = \lim_{t\to\infty} \frac{e^2}{6tVk_BT}\sum_{i,j}^{N} z_i^2\langle([\mathbf{R}_i(t) - \mathbf{R}_i(0)])([\mathbf{R}_j(t) - \mathbf{R}_j(0)])\rangle \quad (4)$$

where e is the electron charge, V is the volume of the simulation box, k_B is Boltzmann's constant, T is the temperature, t is time, z_i and z_j are the charges over ions i and j in electrons, $\mathbf{R}_i(t)$ is the displacement of the ion i during time t, the summation is performed over all ions, $\langle\ \rangle$ denote the ensemble average, and N is the total number of ions in the simulation cell. Here $\lambda^{app}(t)$ is the apparent time-dependent conductivity whose long-time limit corresponds to the equilibrium DC conductivity of an electrolyte with nonblocking electrodes. Determining the long-time limit of $\lambda^{app}(t)$ with eq 4 is problematic even at high temperatures where the diffusion coefficients can be accurately determined because $\lambda^{app}(t)$ has poorer statistics and a higher uncertainty compared to MSD(t).

Conductivity can be decomposed into an "ideal" conductivity that would be realized if ion motion where uncorrelated, denoted $\lambda_{uncorr}(t)$, and the degree to which ion motion is uncorrelated, or α_d. The degree of uncorrelated ion motion is given as the ratio of the collective (total) charge transport (λ) to the charge transport due to self-diffusion only (λ_{uncorr})

$$\lambda^{app}_{uncorr} = \lim_{t\to\infty} \lambda^{app}_{uncorr}(t) = \lim_{t\to\infty} \frac{e^2}{6tVk_BT}\sum_{i}^{N} z_i^2\langle[\mathbf{R}_i(t) - \mathbf{R}_i(0)]^2\rangle = \frac{e^2}{Vk_BT}(n_{Li^+}D^{app}_{Li^+} + n_{TFSI^-}D^{app}_{TFSI^-}) \quad (5)$$

$$\alpha_d = \frac{\lambda}{\lambda_{uncorr}} = \lim_{t\to\infty} \alpha_d(t) = \lim_{t\to\infty} \frac{\lambda^{app}(t)}{\lambda^{app}_{uncorr}(t)}Z \quad (6)$$

Here n_i is the number of atoms of type i = (Li^+ or $TFSI^-$), $n = n_{Li^+} + n_{TFS^-}$. The degree of ion uncorrelated motion $\alpha_d = 1$ corresponds to completely uncorrelated ion motion, while $\alpha_d = 0$ if all of the cations only move together with anions.

The $\alpha_d(t)$ were calculated with eq 6 and are shown in Figure 5 for IL and the binary electrolyte for the time scale where we feel that adequate statistics are present for accurate determination of $\alpha_d(t)$. The time averaged values of α_d from Figure 6 are given in Table 2. We assumed that the α_d values from the subnanosecond regime are similar to those at long times. MD simulations predict α_d for the IL are similar to the values observed for pyrrolidinum$^+$/$TFSI^-$ and imidazolium/$TFSI^-$ ILs from our previous simulations.[40,41] The degree of ion uncorrelated motion for the binary electrolyte EO_{12}/LiTFSI is significantly higher than that for the IL and is in good agreement with estimates from joint conductivity and pgf-NMR experiments for similar electrolytes.[20] For both electrolytes α_d, i.e., the degree of uncorrelated motion, increases with decreasing temperature as previously discussed in details for binary PEO doped with lithium salt.[30] For the EO_{12}/LiTFSI binary electrolyte α_d correlates well with the fraction of solvent-separated ions obtained from structural analysis (α_s, Table 2), indicating that solvent-separated ions move largely independently. This correlation does not hold for the $EO_{12}TFSI^-/Li^+$ ionic liquid. Specifically, the degree of uncorrelated motion (α_d) is significantly lower (ca. a factor of 2) than the fraction of solvent-separated ion pairs (α_s). This discrepancy will be explained below in terms of Li^+ separated from $TFSI^-$ ether oxygen atoms moving together with an oligother chain that is in turn connected to a $TFSI^-$ ion.

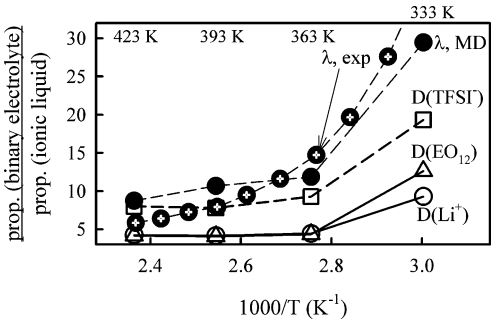

Figure 6. Ratio of the EO_n/LiTFSI self-diffusion coefficient to that in EO_nTFSI^-/Li^+ IL from MD simulations and experiments.

The conductivities of EO_{12}/LiTFSI and $EO_{12}TFSI^-/Li^+$ IL were calculated as $\lambda = \lambda_{uncorr}\alpha_d$ and are compared with experimental data in Figure 1. Good agreement between MD simulations and experiments is observed for both binary electrolyte and the IL, while MD simulations predict slightly lower values than experiments. The deviation of MD predicted conductivities from experimental data is partially due to the finite size of the simulation cell as discussed above for the case of self-diffusion coefficients. The ratio of ion conductivity in binary electrolyte to that in IL from MD simulations and experiment reflects slowing down of charge transport in the IL compared to the binary electrolyte as shown in Figure 6. This ratio increases with decreasing temperature highlighting the stronger temperature dependence of conductivity in the IL in comparison with the binary electrolyte. The decrease in conductivity of IL in comparison to the binary electrolyte is due to dramatic slowing down (a factor of 8−9) of $TFSI^-$ motion due to its attachment to oligoether, slowing down of Li^+ diffusion, and an increased correlation between ions reflected by a decrease of α_d. All of these effects result from the attachment of the $TFSI^-$ anion to EO_{12}.

VI. Microscopic Model of Li^+ Transport

We observe from simulations that Li^+ cations are moving together with approximately four oxygen atoms that are part of EO_{12} or $EO_{12}TFSI^-$, jumping along oligoether chains and hopping from one chain to another. We also observe that Li^+

cations move by complexing/decomplexing $TFSI^-$ or move together with an anion, but such mechanisms do not dominate ion transport because of the high degree of oligoether separated ion pairs as shown in Table 2. Finally, in EO_{12}/LiTFSI a Li^+ cation is likely to move together with an EO_{12} chain and contribute to charge transport, while such motion in $EO_{12}TFSI^-/Li^+$ IL is not going to result in any charge transport. To quantify contribution to the total Li^+ transport from each mechanism and understand interrelations between them, we have idealized complex mechanisms of ion transport by taking into account only the most important contributions and incorporated them in a microscopic model[26] that was successfully applied to obtain fundamental understanding of Li^+ motion in high molecular weight PEO.

The microscopic model has been previously[26] described in detail; however, we briefly describe it here for completeness. In the model an ensemble of cations occupying coordinating sites on oligoether chains is simulated via Monte-Carlo moves. Each Li^+ occupies 4 coordination sites corresponding to the closely coordinated ether oxygen atoms on a one-dimensional lattice. Each Li^+ is allowed to move (jump) along chains containing 12 coordination sites mimicking EO_{12} with a jumping rate r_{jump} [ns^{-1}] and hop from a chain to another chain with a characteristic hopping length of 6 Å taken from our previous work on PEO/LiTFSI[26] after residing with a chain for time $\tau_{Li^+-chain}$. A relationship between the average physical distance between any atoms i and j (R_{ij}) of the same oligoether chain and the number of bonds ($|i - j|$) comprising the chain segment between these atoms is established by the Gaussian chain statistics

$$\langle R_{ij}^2 \rangle = C|i - j|l^2 \tag{7}$$

where l^2 is the mean-squared bond length (2.07 $Å^2$) and C_n ($n = |i - j|$) is the characteristic ratio of PEO that depends on n. Each coordination site is separated by three bonds. Motion along the polymer chains as well as interchain hopping are carried out utilizing Monte-Carlo moves. The Li^+ motion together with a coordination shell of 4 ether oxygen atoms (coordination cites) is characterized by an $MSD^{LiCoord}(t)$ and is included in the model.

We quantified the residence time for a Li^+ cation to be coordinated by a oligoether chain or by an EO group by calculating the lifetime autocorrelation function (ACF) $P(t)$ for Li^+-chain and Li^+-EO that are formally defined as:

$$P(t) = \frac{\langle H_{ij}(t)H_{ij}(0)\rangle}{\langle H_{ij}(0)H_{ij}(0)\rangle} \tag{8}$$

where for the Li^+-chain ACF $H_{ij}(t)$ is 1 if the ith Li^+ is coordinated by at least two ether oxygen atoms from the jth chain (chain = EO_{12} or $EO_{12}TFSI^-$) and zero otherwise, and for the Li^+-EO ACF $H_{ij}(t)$ is 1 if the ith is coordinated by the jth EO and zero otherwise. The $\langle\ \rangle$ sign denotes average over all time origins and pairs of Li^+-EO or Li^+-chain pairs (chain = EO_{12} or $EO_{12}TFSI^-$). An example of the Li^+-EO and Li^+-chain residence time ACFs is shown in Figure 7. The Li^+-chain ACF exhibits a single-exponential decay $\exp(-t/\tau_{Li^+-chain})$. We fitted $\tau_{Li^+-chain}$ to MD simulation data as shown in Figure 7. The resulting $\tau_{Li^+-chain}$ residence times for EO_{12}/LiTFSI and $EO_{12}TFSI^-/Li^+$ are shown in Figure 8. The rate of Li^+ interchain hopping is slower in $EO_{12}TFSI^-/Li^+$ IL compared to EO_{12}/LiTFSI by a factor of about 2 with the difference increasing slightly as temperature decreases.

Next the Li^+-EO residence time ACF was calculated with eq 7 and is shown in Figure 7. It exhibits stretched exponential

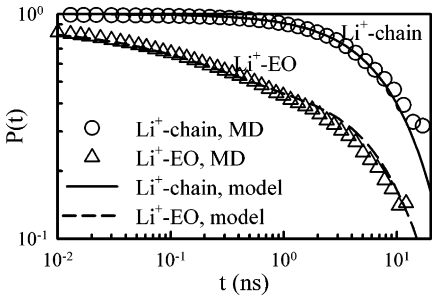

Figure 7. The Li^+-chain and Li^+-EO residence time ACF for EO_{12}/LiTFSI binary electrolyte at 423 K from MD simulations and from microscopic model fits. $P(t)$ from the model was scaled by 0.85 to match response on a picosecond time scale not described by the microscopic model.

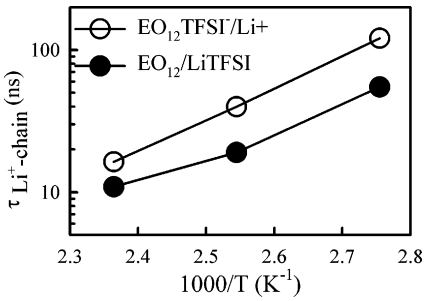

Figure 8. The Li^+-chain residence time for EO_{12}/LiTFSI binary electrolyte and $EO_{12}TFSI^-/Li^+$ IL from MD simulations.

behavior, i.e., $\exp[-(t/\tau)^\beta]$, with $\beta \approx 0.3$. The highly stretched exponential behavior is associated with a Li^+ moving away from an EO coordination site and returning back multiple times before hopping to another chain as observed from visualization of the Li^+ motion along oligoether chains. The jumping rate r_{jump} for the Li^+ motion along an oligomer chain was varied to obtain the best agreement between the model and MD data as shown in Figure 7 while keeping $\tau_{Li^+-chain}$ fixed. The EO jumping rate r_{jump} determines the initial decay of the Li^+-EO ACF, while $\tau_{Li^+-chain}$ determines its terminal relaxation. Indeed, if no interchain jumps are allowed the Li^+-EO ACF will saturate at a constant value determined by the length of the chain. The jumping rates are summarized in Table 2. The rate of intrachain jumping (r_{jump}) is somewhat higher in EO_{12}/LiTFSI than in the $EO_{12}TFSI^-/Li^+$ IL.

The final parameter needed for the microscopic model is the $MSD^{LiCoord}(t)$, i.e., the time-dependent MSD for a Li^+ cation moving while not exchanging the ether oxygen atoms coordinating it. $MSD^{LiCoord}(t)$ is shown in Figure 9. In a process of calculating $MSD^{LiCoord}(t)$ we allowed a change in a Li^+ coordination by one EO to extend the time range for which we have good statistics for $MSD^{LiCoord}(t)$. The $MSD^{LiCoord}(t)$ is only slightly lower than the total Li^+ MSD(t) on a time scale <10 ns indicating that the Li^+ motion with its coordination shell is a dominant contribution to the local (short-time) motion of the cation for PEO_{12}/LiTFSI. Figure 9 indicates that reliable $MSD^{LiCoord}(t)$ data exist only for up to 10 ns for 423 K, which is not long enough to parametrize the microscopic model. To extend the range of the $MSD^{LiCoord}(t)$ we assumed that the $MSD^{LiCoord}(t)$ is equal to the MSD(t) for EO_{12} or $EO_{12}TFSI^-$ center of mass for long times. This assumption does not significantly influence model predictions because a Li^+ cation typically hops to another chain by this time.

Predictions of the macroscopic model for MSD(t) of Li^+ cation are compared with MD simulation data in Figure 3. Good agreement between the model and MD data validates the model.

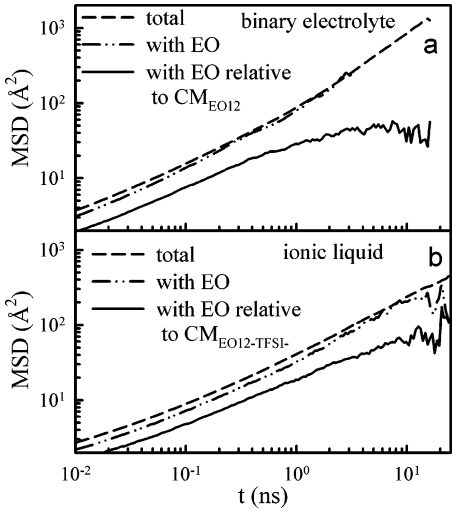

Figure 9. The total Li^+ mean-square displacement (MSD), the MSD for Li^+ motion with its coordination shell of ether oxygens (EO), and the MSD for Li^+ motion with its coordination shell of EOs relative to the chain center of mass from MD simulations.

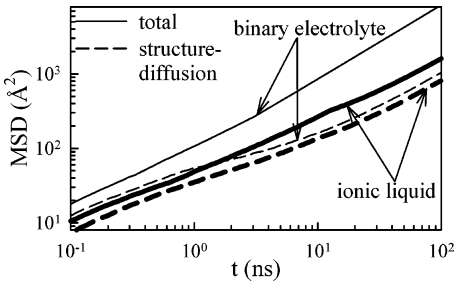

Figure 10. Total Li^+ MSD and structure-diffusion Li^+ MSD for EO_{12}/LiTFSI binary electrolyte and $EO_{12}TFSI^-/Li^+$ IL at 423 K from the microscopic model.

The microscopic model allows us to separate vehicular (motion together with a chain) and the remaining (structure-diffusion) contribution to the total Li^+ motion. Thus, the structure-diffusion contribution, which includes Li^+ jumping along the chain, is its motion with a segment of the chain relative to the chain center of mass (also shown in Figure 9) and hopping from one chain to another. The microscopic model prediction of the structure-diffusion contribution to the total Li^+ transport is shown in Figure 10. For the binary electrolyte, where the similarity in self-diffusion coefficient of Li^+ and the oligoether solvent EO_{12} (Figure 4a) would imply the dominance of vehicular motion, the structure-diffusion mechanism is responsible for only 10% of the Li^+ transport in the EO_{12}/LiTFSI binary electrolyte. In contrast, the structure-diffusion mechanism in the $EO_{12}TFSI^-/Li^+$ IL contributes approximately half of the Li^+ transport with the remainder coming from Li^+ diffusion together with $EO_{12}TFSI^-$ chains. The latter (vehicular) contribution corresponds to the motion of neutral species ($EO_{12}TFSI^-/Li^+$ pair) that does not contribute to macroscopic charge transport. Motion of a Li^+ cation with an (anionic) oligoether in the IL results in correlated motion of anion and cation even though the Li^+ and oligoether-attached $TFSI^-$ are not directly bound. In contrast, in the binary electrolyte, motion of a Li^+ cation with a (neutral) oligoether does lead to net charge transport and does not lead (necessarily) to correlated ion motion. As a result, the degree of uncorrelated ion motion in the binary liquid is greater than that in the binary electrolyte as was shown in Figure 5.

An interesting observation from Figure 10 is that the structure-diffusion contribution to Li^+ transport in both the binary electrolyte and the IL is very similar. The minor difference comes from the slower rate of interchain hopping shown in Figure 8 and the slower local relaxation (motion along the chain and with a coordinating oligoether segment observed in the IL). Interestingly, local conformational relaxation of IL has a slightly stronger temperature dependence than local relaxation of binary electrolytes. As this relaxation is expected to be coupled to both Li^+ local transport and interchain hopping rate, it is likely to underline the stronger temperature dependence of conductivity of IL vs binary electrolytes.

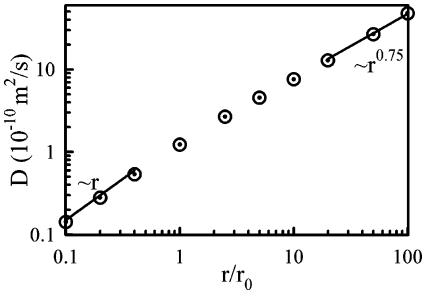

Figure 11. Dependence of the Li^+ structure-diffusion coefficient on the rate of interchain hopping r normalized to the rate r_0 from Table 2 for $EO_{12}TFSI^-/Li^+$ IL at 423 K.

The microscopic model also allows us to probe the contribution from the Li^+ jumping along the chain to the total Li^+ transport. Turning off Li^+ motion along the oligoether reduces the Li^+ structure-diffusion coefficient by ~25% for both EO_{12}/LiTFSI and $EO_{12}TFSI^-/Li^+$ electrolytes.

One of the most intriguing questions is if it is possible to predict the behavior of ionic liquid with an attached anion from simulations of a binary electrolyte. The structure-diffusion determines the Li^+ diffusion relative to the $EO_{12}TFSI^-$ chain and, thus, conductivity of IL. Figure 10 suggests that the structure-diffusion contribution is similar to both IL and the binary electrolyte at least for high temperature. Therefore, if one knows the structure-diffusion in a binary electrolyte one can obtain approximate conductivity in IL. This approximation is expected to become even better for lower salt concentrations because a smaller fraction of a polymer chain is influenced by attaching an anion. However, Figure 8 indicates that the interchain hopping rates become more dissimilar as temperature decreases and the ratio of $MSD^{LiCoord}(t)$ for EO_{12}/LiTFSI to that for $EO_{12}TFSI^-/Li^+$ increases from 2.2 to 3 as temperature decreases from 423 to 363 K. This suggests that the structure-diffusion contributions for EO_{12}/LiTFSI and $EO_{12}TFSI^-/Li^+$ deviate from each other as temperature decreases.

A. Bottleneck for the Li^+ Transport in $EO_{12}TFSI^-/Li^+$ Ionic Liquid. It is important to understand what the bottleneck for Li^+ diffusion in IL is in order to guide strategies for improving IL conductivity. Both local Li^+ cation motion, represented by Li^+ motion along the oligoether chain and motion of the coordinating oligoether segment relative to the chain center of mass, and the interchain hopping rate influence Li^+ mobility in the IL. One can think about Li^+ transport as Li^+ moving around a cage with a size given approximately by chain radius of gyration R_g and hopping to another cage with the characteristic time of $\tau_{Li^+-chain}$. This is in line with ideas of the dynamic bond percolation (DBP) theory.[42] The dependence of the Li^+ structure-diffusion coefficient on the interchain hopping rate for the case where the local Li^+ mobility is kept constant is shown in Figure 11. A decrease of the hopping rate leads to an almost linear decrease of the Li^+ diffusion coefficient indicating that in this regime the Li^+ motion is completely determined and thus limited by the interchain hopping rate. One

can rationalize this behavior by comparing characteristic time scales for the $EO_{12}TFSI^-$ chain motion with the time scale for interchain hopping. The Rouse time for $EO_{12}TFSI^-$ characterizing its global reorientation is ~4.4 ns at 423 K. After this time Li^+ motion relative to the $EO_{12}TFSI^-$ center of mass saturates (so-called "cage" is explored in terms of DBP theory), while the time scale for interchain hopping is 18 ns, which is 4 times larger than the time scale for chain reorientation. Thus, increasing the local Li^+ motion (e.g., time to explore the "cage") will not significantly influence Li^+ long time diffusion because the "cage" has already been explored multiple times before an interchain jump occurs. Increasing the interchain hopping rate eventually leads to the regime where the lithium diffusion does not scale linearly with the interchain hopping rate; we observe $D^{Li^+} \approx r^{0.75}$ as shown in Figure 11. The absence of linear scaling implies the dependence of the Li^+ structure-diffusion coefficient on factors other than the Li^+ interchain hopping. The only other factor present in the model is the Li^+ local relaxation represented by the Li^+ motion along the chain and with the segment. Thus, in this regime $(r/r_0) \gg 1$ the Li^+ motion inside the cage and that hopping from cage to cage are both important if the process is thought of in terms of DBP theory.

At the end of this discussion we would like to comment on molecular weight dependence of the model. Doubling the degree of polymerization of oligoether in IL from 12 to 24 increases Rouse time for chain reorientation by a factor of 4 making it comparable to the interchain hopping rate assuming the later one does not change. This puts us in the regime when both local relaxation and interchain hopping rate are important for the Li^+ structure-diffusion.

VII. Conclusions

MD simulations were performed on the EO_{12}/LiTFSI binary electrolyte and $EO_{12}TFSI^-/Li^+$ IL. The conductivity of EO_{12}/LiTFSI and $EO_{12}TFSI^-/Li^+$ from MD simulations is in good agreement with the experimentally measured values. Attaching the $TFSI^-$ anion to the chain end of the oligoether resulted in reduction of conductivity by 1 order of magnitude at 423 K and 2 orders of magnitude at room temperature. The Li^+ cations were found to be separated from the $TFSI^-$ anion by oligoether in most instances (75−90%) for both EO_{12}/LiTFSI and $EO_{12}TFSI^-/Li^+$. For the EO_{12}/LiTFSI electrolyte, the fraction of separated $Li^+/TFSI^-$ ions is similar to the degree of ion uncorrelated motion, while for the IL a degree of ion uncorrelated motion was significantly lower (~45−55%) than the fraction of separated $Li^+/TFSI^-$.

The Li^+ cation self-diffusion coefficient in binary EO_{12}/LiTFSI electrolyte was dominated (90%) by Li^+ vehicular diffusion of the Li^+ with an EO_{12} solvent. In IL half of the Li^+ motion was attributed to the Li^+ motion with the $EO_{12}TSFI^-$ anion, with the other half being due to the structure-diffusion that involves a Li^+ local motion along the chain, Li^+ motion together with its coordination shell, and interchain hopping. Only structure-diffusion contributes to charge transport in ILs, as vehicular motion results in transport of neutral species accounting for reduction of conductivity by a factor of 2. Interestingly, structure-diffusion of the Li^+ cation in the binary electrolyte (EO_{12}/LiTSFI) is quite similar to that in $EO_{12}TFSI^-/Li^+$ ionic liquid. However, as temperature decreases the Li^+ structure-diffusion in IL becomes slower than that in the binary electrolyte. Finally, Li^+ diffusion in the $EO_{12}TFSI^-/Li^+$ ILs was found to be limited by the Li^+ interchain hopping as opposed to local Li^+ relaxation comprised from Li^+ local motion along the chain, Li^+ motion together with its coordination shell.

Acknowledgment. The authors are grateful for financial support of this work by the Assistant Secretary for Energy Efficiency and Renewable Energy, Office of FreedomCAR and Vehicle Technologies of the U.S. Department of Energy under Contract No. DE-AC02-05CH11231 on PO No. 6515401 (University of Utah) and PO No. 6515399 (Clemson University).

References and Notes

(1) Tarascon, J. M.; Armand, M. *Nature* **2001**, *414* (6861), 359−367.

(2) Shin, J. H.; Henderson, W. A.; Passerini, S. *Electrochem. Solid State Lett.* **2005**, *8* (2), A125−A127.

(3) Shin, J.-H.; Henderson, W. A.; Tizzani, C.; Passerini, S.; Jeong, S.-S.; Kim, K.-W. *J. Electrochem. Soc.* **2006**, *153* (9), A1649-A1654.

(4) Doyle, M.; Fuller, T. F.; Newman, J. *Electrochim. Acta* **1994**, *39* (13), 2073−2081.

(5) Trapa, P. E.; Acar, M. H.; Sadoway, D. R.; Mayes, A. M. *J. Electrochem. Soc.* **2005**, *152* (12), A2281−A2284.

(6) Allcock, H. R.; Welna, D. T.; Maher, A. E. *Solid State Ionics* **2006**, *177* (7−8), 741−747.

(7) Sun, X. G.; Hou, J.; Kerr, J. B. *Electrochim. Acta* **2005**, *50* (5), 1139−1147.

(8) Sun, X. G.; Reeder, C. L.; Kerr, J. B. *Macromolecules* **2004**, *37* (6), 2219−2227.

(9) Zhang, S. H.; Dou, S. C.; Colby, R. H.; Runt, J. *J. Non-Cryst. Solids* **2005**, *351* (33−36), 2825−2830.

(10) Hallac, B. B.; Geiculescu, O. E.; Rajagopal, R. V.; Creager, S. G.; DesMarteau, D. D. *J. Electrochem. Soc.* Submitted for publication.

(11) Watanabe, M.; Suzuki, Y.; Nishimoto, A. *Electrochim. Acta* **2000**, *45* (8−9), 1187−1192.

(12) Siska, D. P.; Shriver, D. F. *Chem. Mater.* **2001**, *13* (12), 4698−4700.

(13) Ito, K.; Nishina, N.; Ohno, H. *J. Mater. Chem.* **1997**, *7* (8), 1357−1362.

(14) Chauvin, C.; Ollivrin, X.; Alloina, F.; LeNest, J. F.; Sanchez, J. Y. *Electrochim. Acta* **2005**, *50* (19), 3843−3852.

(15) Ito, K.; Tominaga, Y.; Ohno, H. *Electrochim. Acta* **1997**, *42* (10), 1561−1570.

(16) Tominaga, Y.; Ito, K.; Ohno, H. *Polymer* **1997**, *38* (8), 1949−1951.

(17) Tominaga, Y.; Ohno, H. *Solid State Ionics* **1999**, *124* (3−4), 323−329.

(18) Tominaga, Y.; Ohno, H. *Chem. Lett.* **1998**, (9), 955−956.

(19) Tominaga, Y.; Ohno, H. *Electrochim. Acta* **2000**, *45* (19), 3081−3086.

(20) Hayamizu, K.; Akiba, E.; Bando, T.; Aihara, Y. *J. Chem. Phys.* **2002**, *117* (12), 5929−5939.

(21) Ayyagari, C.; Bedrov, D.; Borodin, O.; Smith, G. D. *Lucretius*, MD simulation code; University of Utah: Salt Lake City, Utah; http://lucretius.mse.utah.edu/.

(22) Borodin, O.; Smith, G. D. *J. Phys. Chem. B* **2006**, *110* (12), 6279−6292.

(23) Borodin, O.; Smith, G. D. *J. Phys. Chem. B* **2006**, *110* (12), 6293−6299.

(24) Frenkel, D.; Smit, B. *Understanding Molecular Simulation*: *From Algorithms to Applications*, 2nd ed.; Academic Press: New York, 2002.

(25) Martyna, G. J.; Tuckerman, M.; Tobias, D. J.; Klein, M. L. *Mol. Phys.* **1996**, *87* (5), 1117−1157.

(26) Borodin, O.; Smith, G. D. *Macromolecules* **2006**, *39* (4), 1620−1629.

(27) Mao, G. M.; Saboungi, M. L.; Price, D. L.; Armand, M. B.; Howells, W. S. *Phys. Rev. Lett.* **2000**, *84* (24), 5536−5539.

(28) Henderson, W. A.; McKenna, F.; Khan, M. A.; Brooks, N. R.; Young, V. G.; Frech, R. *J. Phys. Chem. B* **2005**, *17*, 2284−2289.

(29) Edman, L. *J. Phys. Chem. B* **2000**, *104* (31), 7254−7258.

(30) Borodin, O.; Smith, G. D. *Macromolecules* **1998**, *31* (23), 8396−8406.

(31) Borodin, O.; Smith, G. D.; Douglas, R. *J. Phys. Chem. B* **2003**, *107* (28), 6824−6837.

(32) Borodin, O.; Smith, G. D.; Jaffe, R. L. *J. Comput. Chem.* **2001**, *22* (6), 641−654.

(33) Siqueira, L. J. A.; Ribeiro, M. C. C. *J. Chem. Phys.* **2005**, *122* (19), 194911.

(34) Xu, K. *Chem. Rev.* **2004**, *104* (10), 4303−4417.
(35) Nowinski, J. L.; Lightfoot, P.; Bruce, P. G. *J. Mater. Chem.* **1994**, 4, 1579−1580.
(36) Borodin, O.; Smith, G. D.; Henderson, W. *J. Phys. Chem. B* **2006**, *110*, 16879−16886.
(37) Borodin, O.; Smith, G. D. *J. Phys. Chem. B* **2006**, *110* (10), 4971−4977.
(38) Gejji, S. P.; Suresh, C. H.; Babu, K.; Gadre, S. R. *J. Phys. Chem. A* **1999**, *103* (37), 7474−7480.
(39) Dunweg, B.; Kremer, K. *J. Chem. Phys.* **1993**, *99* (9), 6983−6997.
(40) Borodin, O.; Smith, G. D. *J. Phys. Chem. B* **2006**, *110*, 11481−11490.
(41) Tokuda, H.; Hayamizu, K.; Ishii, K.; Abu Bin Hasan Susan, Md.; Watanabe, M. *J. Phys. Chem. B* **2004**, *108* (42), 16593−16600.
(42) Snyder, J. F.; Ratner, M. A.; Shriver, D. F. *J. Electrochem. Soc.* **2001**, *148* (8), A858−A863.